Bull Earthquake Eng (2015) 13:1183–1203
DOI 10.1007/s10518-014-9692-z

ORIGINAL RESEARCH PAPER

Bayesian Cloud Analysis: efficient structural fragility assessment using linear regression

Fatemeh Jalayer · Raffaele De Risi · Gaetano Manfredi

Received: 28 February 2014 / Accepted: 6 October 2014 / Published online: 21 October 2014

Abstract Cloud Analysis is based on simple regression in the logarithmic space of structural response versus seismic intensity for a set of registered records. A Bayesian take on the Cloud Analysis, presented herein, manages to take into account both record-to-record variability and other sources of uncertainty related to structural modelling. First, the structural response to a suite of ground motions, applied to different realizations of the structural model generated through a standard Monte Carlo, is obtained. The resulting suite of structural response is going to be used as "data" in order to update the joint probability distribution function for the two regression parameters and the conditional logarithmic standard deviation. In the next stage, large-sample MC simulation based on the updated joint probability distribution is used to generate a set of plausible fragility curves. The robust fragility is estimated as the average of the generated fragility curves. The dispersion in the robust fragility is estimated as the variance of the plausible fragility curves generated. The plus/minus one standard deviation confidence interval for the robust fragility depends on the size of the sample of "data" employed. Application of the Bayesian Cloud procedure for an existing RC frame designed only for gravity-loading demonstrates the effect of structural modelling uncertainties, such as the uncertainties in component capacities and those related to construction details. Moreover, a comparison of the resulting robust fragility curves with fragility curves obtained based on the Incremental Dynamic Analysis shows a significant dependence on both the structural performance measure adopted and the selection of the records.

Keywords Seismic risk · Structural reliability · Performance-based assessment · Robust fragility · Modelling uncertainties · Simulation methods · Engineering demand parameter

F. Jalayer (✉) · R. De Risi · G. Manfredi
Department of Structures for Engineering and Architecture, University of Naples Federico II, Via Claudio 21, 80125 Naples, Italy
e-mail: fatemeh.jalayer@unina.it

1 Introduction

Analytic structural fragility assessment is one of the fundamental steps in the modern performance-based engineering (Cornell and Krawinkler 2000). The structural fragility can be defined as the conditional probability of exceeding a prescribed limit state given the intensity measure (IM). If the structural limit state is expressed in terms of one or more engineering demand parameters (EDPs), the fragility is going to depend significantly on the EDP-IM relationship. There are alternative non-linear dynamic analysis procedures available in the literature for characterizing the relationship between EDP and IM based on recorded ground motions, such as, the Incremental Dynamic Analysis (IDA, Vamvatsikos and Cornell 2002), Multiple-Stripe Analysis (MSA, Bazzurro et al. 1998; Jalayer and Cornell 2009; Baker 2007) and the Cloud Method (Bazzurro et al. 1998; Shome et al. 1998; Luco and Cornell 1998; Jalayer 2003), just to name a few. The nonlinear dynamic methods such as IDA and MSA are suitable for evaluating the relationship between the EDP and the IM for a wide range of IM values. The application of MSA and IDA can sometimes be quite time-consuming as the non-linear dynamic analyses are going to be repeated (usually for scaled ground motion time-histories) for increasing levels of ground motion intensity. The Cloud Method is particularly efficient since it involves the non-linear analysis of the structure subjected to a set of un-scaled ground motion time-histories. The simplicity of its underlying formulation makes it a quick and efficient analysis procedure for fragility assessment or safety-checking in the context of the SAC-FEMA formulation (Cornell et al. 2002). The Cloud Method has been used, not only to model the record-to-record variability in ground motion, but also to propagate structural modelling uncertainties such as uncertainty in component capacity (Jalayer et al. 2007) and the uncertainties in mechanical material properties and construction details (Jalayer et al. 2011a). Furthermore, a modified version of the Cloud Method has been proposed in (Elefante et al. 2010) that implements a weighting scheme for taking into account magnitude and shape-factor dependence conditioned on the adopted IM. An information-based relative measure for the sufficiency (Luco and Cornell 2007) of the adopted IM has been derived based on Cloud Method's underlying probabilistic model in (Jalayer et al. 2012). The efficiency and simplicity of the Cloud Method can also be exploited in order to estimate the cumulative damage caused by a sequence of aftershocks through back-to-back or sequential Cloud Analysis (Jalayer et al. 2011b; Ebrahimian et al. 2014).

The Cloud Method has several limitations such as the assumption of a constant conditional standard deviation for probability distribution of the EDP given IM. Arguably, with the increasing levels of the IM, the conditional dispersion in displacement-based EDP's given IM may increase (see e.g., Vamvatsikos and Cornell 2002; Jalayer and Cornell 2009). Another short-coming of the method is its strong dependence on the suite of ground motion records. For example, the resulting regression prediction (and also its dispersion) can change as a function of the range of ground motion intensities spanned by the selected records (Jalayer 2003). The Cloud Method has been used primarily for taking into account the uncertainties related to the ground motion representation also known as the record-to-record variability. There has been efforts in taking into account in an approximate manner the so-called "epistemic" uncertainties (as distinct from record-to-record variability, roughly speaking) in Cornell et al. (2002), Jalayer and Cornell (2003), and Jalayer et al. (2007), to name a few. The effect of the epistemic uncertainties in these works is represented in the form of an overall increase in the dispersion for the probability of exceeding the limit state. However, they do not manage to capture the bias in median limit state probability due the effect of epistemic uncertainties. In the recent years, several alternative methods have been proposed that

combine reliability methods such as the first order second moment (FOSM, see for example Melchers 1999) methods or simulation-based methods (e.g., Monte Carlo) with non-linear dynamic procedures such as IDA in order to take into account also sources of uncertainties other than record-to-records variability, based on recorded ground motions (Dolsek 2009; Vamvatsikos and Fragiadakis 2010; Celarec and Dolšek 2013). Alternatively, Liel et al. 2009 have proposed combining the Monte Carlo simulation and response surface method (a time-invariant reliability method based on sensitivity analysis) and incremental dynamic analysis in order to take into account various sources of uncertainties. The Bayesian Cloud Method discussed herein builds on a method presented in a preliminary form in Jalayer et al. 2011a in which Cloud Analysis and Monte Carlo simulation were combined in a Bayesian framework in order to take into account both the structural modelling uncertainties and record-to-record variability.

In particular, well-established results in Bayesian parameter estimation (see e.g., Box and Tiao 1992) are going to be used herein in order to construct an analytic closed-form (posterior) joint probability distribution for parameters of a regression-based Log Normal fragility model. In doing so, the results of the Cloud Analysis expressed in terms of a (limited) set of EDP values, obtained by applying a suite of records to various realizations of the structural model –taking into account structural modelling uncertainties– are going to be used as "data". A "robust" (e.g., Papadimitriou et al. 2001; Jalayer et al. 2010) estimate of the structural reliability can be obtained by integrating the Log Normal structural fragility model and the joint probability distribution for the analytic fragility parameters. Solving the integral using Monte Carlo simulation, leads to the estimation of the robust fragility and its plus/minus one standard deviation confidence interval. The results are going to be compared with those obtained by employing the incremental dynamic analysis, for a shear-critical moment resisting frame belonging to an existing school building designed for gravity loading only (in its pre-retrofit state).

2 Choice of performance variable and IM

The small-amplitude first-mode spectral acceleration denoted by $S_a(T_1)$ or simply S_a is adopted as the IM. This intensity measure has been proved to be a relatively sufficient intensity measure for moment-resisting frames with first-mode periods lying within the moderate range (see e.g., Shome et al. 1998; Jalayer et al. 2012). The engineering demand parameter and/or decision variable herein is taken to be the critical demand to capacity ratio denoted as Y_{LS} and defined as the demand to capacity ratio for the component that brings the system closer to the onset of limit state LS[1]. The formulation is based on the cut-set concept (Ditlevsen and Madsen 1996), which is suitable for cases where various potential failure mechanisms can be defined a priori:

$$Y_{LS} = \max_{l}^{N_{mech}} \min_{j}^{N_l} \frac{D_{jl}}{C_{jl}(LS)} \tag{1}$$

where N_{mech} is the number of considered potential failure mechanisms and N_l the number of components taking part in the lth mechanism. D_{jl} is the demand evaluated for the jth component of the lth mechanism and $C_{jl}(LS)$ is the limit state capacity for the jth component of the lth mechansim. In the context of system reliability, a cut set is defined as any set of components whose joint failure $Y(l) = \min D_{jl}/C_{jl} > 1$, implies

[1] Y_{LS} could also be considered a decision variable since the performance objective and the limit state are both defined as a function of this variable.

failure of the system, $Y = \max Y(l) > 1$. It should be noted that the cut-sets can be defined in a systematic manner and similar to how one defines which actions to read after doing structural analysis. One of the advantages of the decision variable Y_{LS} is that it manages to relate the structural behaviour at the component level to its global performance.

In particular, two different sets of decision variables, based on the cut-set concept, have been considered in this work; namely, the deformation-based critical demand to capacity ratio denoted as Y_{LS-D} and the overall Y_{LS}. The deformation-based critical demand to capacity ratio denoted as Y_{LS-D} takes into account only the failure mechanisms related to the chord rotation in the beam-column members. On the other hand, the overall Y_{LS} takes into account also brittle failure modes such as shear failure in the structural members. Such formulation is particularly useful in cases where the non-linear shear behavior is not modeled explicitly at the element level.

Finally, and for the sake of comparison, the maximum inter-story drift ratio (MIDR or later θ_{max}) is adopted also as an EDP. The maximum inter-story drift ratio is a widely-used global EDP for moment-resisting frames. Arguably, it is able to relate the excessive rotations on the element level to the global deformation of the structure (Jalayer and Cornell 2009). Therefore, it is expected to see a reasonable correlation between Y_{LS-D} and MIDR. In order to render MIDR more compatible with the EDP's based on the cut-set formation (i.e., defined as a critical demand to capacity ratio), it is also normalized by the MIDR at the threshold of the limit state obtained through the static pushover analysis. Although the methodological proposal is general with respect to the choice of the limit state *LS*, the focus of this work is on the collapse or global instability limit state.

3 A brief overview of the Cloud Analysis

The Cloud Analysis implements the non-linear dynamic analysis results in a (linear) regression-based probabilistic model. Let $D = \{Y_i,\ i = 1{:}N\}$ be the critical demand to capacity ratio calculated through non-linear time-history analysis performed for a suite of N recorded ground motions with $\boldsymbol{S}_a = \{S_{a,i},\ i = 1{:}N\}$. The probabilistic model can be described as following:

$$E\left[\log Y \mid S_a\right] = \log \eta_{Y|S_a} = \log a + b \log S_a$$
$$\sigma_{\log Y|S_a} = \sqrt{\frac{\sum_{i=1}^{n} \left(\log Y_i - \log \eta_{Y|S_{a,i}}\right)^2}{n-2}} \tag{2}$$

where $\eta_{Y|Sa}$ is the median for Y given S_a and $\sigma_{\log Y|Sa}$ is the logarithmic standard deviation for Y given S_a. The structural fragility obtained based on the Cloud Method can be expressed as:

$$P(Y > 1|\, S_a) = P(\log Y > 0|\, S_a) = 1 - \Phi\left(\frac{-\log \eta_{Y|S_a}}{\sigma_{\log Y|S_a}}\right) = \Phi\left(\frac{\log \eta_{Y|S_a}}{\sigma_{\log Y|S_a}}\right) \tag{3}$$

Note that this is a three-parameter fragility model whose model parameters can be denoted as $\chi = [\log a, b, \beta_{Y|Sa}]$ where $\beta_{Y|Sa} = \sigma_{\log Y|Sa}$.

4 The robust fragility

The robust fragility definition employed here is based on the concept of updated robust reliability in the Bayesian probabilistic framework. The updated robust reliability (Papadimitriou et al. 2001; Beck and Au 2002; Jalayer et al. 2010), denoted as $P(LS|\boldsymbol{D},\boldsymbol{M})$ and conditioned on prescribed modelling assumptions $\boldsymbol{M}$, can be defined as the probability of failure $P(LS|\boldsymbol{\chi},\boldsymbol{D},\boldsymbol{M})$ for a given set of model parameters $\boldsymbol{\chi}$ integrated over the joint (posterior) probability distribution of the model parameters denoted as $p(\boldsymbol{\chi}|\boldsymbol{D},\boldsymbol{M})$ and conditioned on a set of data denoted by $\boldsymbol{D}$. In other words, the "robustness" of this estimate comes from the fact that it takes into account the uncertainty in the parameters of a prescribed probability model $\boldsymbol{M}$ conditioned on data $\boldsymbol{D}$:

$$P\left(LS|\,\mathbf{D},\mathbf{M}\right)=E_{\chi}\left[P\left(LS|\,\mathbf{D},\mathbf{M},\boldsymbol{\chi}\right)\right]=\int_{\Omega(\boldsymbol{\chi})}P\left(LS|\,\boldsymbol{\chi},\mathbf{D},\mathbf{M}\right)\cdot p\left(\boldsymbol{\chi}|\,\mathbf{D},\mathbf{M}\right)\cdot d\boldsymbol{\chi} \quad (4)$$

where $\mathbf{E}_{\boldsymbol{\chi}}[.]$ is the expected value operator over the vector of parameters $\boldsymbol{\chi}$ and $\boldsymbol{\Omega}$ is the domain of vector $\boldsymbol{\chi}$. The result is presented as robust and updated failure probability $P(LS|\boldsymbol{D},\boldsymbol{M})$ given the set of data $\boldsymbol{D}$. Hereafter, the conditioning on the modelling assumptions $\boldsymbol{M}$ is dropped for the sake of simplicity. Inspired from the concept of updated robust reliability, the *robust fragility* is defined as the expected value for a prescribed fragility model taking into account the joint probability distribution for the (fragility) model parameters (Jalayer et al. 2011a). For the fragility model described in Eq. 3, the robust fragility can be written as:

$$P\left(Y>1|\,S_a,\mathbf{D}\right)=E_{\chi}\left[P\left(Y>1|\,S_a,\mathbf{D},\boldsymbol{\chi}\right)\right]=\int_{\Omega(\boldsymbol{\chi})}\Phi\left(\frac{\log\eta_{Y|S_a}}{\beta_{Y|S_a}}\right)\cdot p\left(\boldsymbol{\chi}|\,\mathbf{D}\right)\cdot d\boldsymbol{\chi} \quad (5)$$

where $\boldsymbol{\chi}=[\log a,\ b,\ \beta_{Y|Sa}]$ is the vector of Log Normal fragility model parameters and $p(\boldsymbol{\chi}|\boldsymbol{D})$ is the posterior joint probability distribution for fragility model parameters given the vector of EDP values $\boldsymbol{D}$. The variance σ^2 in fragility estimation can be calculated as:

$$\begin{aligned}\sigma_{\chi}^{2}\left[P\left(Y>1|\,S_a,\boldsymbol{\chi},\mathbf{D}\right)\right]&=E_{\chi}\left[P\left(Y>1|\,S_a,\boldsymbol{\chi},\mathbf{D}\right)-P\left(Y>1|\,S_a,\mathbf{D}\right)\right]^2\\&=\int_{\Omega(\boldsymbol{\chi})}\left[\Phi\left(\frac{\log\eta_{Y|S_a}}{\beta_{Y|S_a}}\right)-P\left(Y>1|\,S_a,\mathbf{D}\right)\right]^2\cdot p\left(\boldsymbol{\chi}|\,\mathbf{D}\right)\cdot d\boldsymbol{\chi}\end{aligned} \quad (6)$$

The joint probability distribution for $\boldsymbol{\chi}$ can be written as (using the probability theory's product rule, Jaynes 2003):

$$p\left(\boldsymbol{\chi}|\,\mathbf{D}\right)=p\left(\log a,b|\,\beta_{Y|S_a},\mathbf{D}\right)p\left(\beta_{Y|S_a}|\,\mathbf{D}\right) \quad (7)$$

In the following, we describe how the probability distributions $\mathrm{p}(\beta_{Y|Sa}|\boldsymbol{D})$ and $\mathrm{p}(\log a, b|\beta_{Y|Sa},\boldsymbol{D})$ are derived (Box and Tiao 1992). The posterior probability distribution for $\beta_{Y|Sa}$ can be calculated as a derived distribution based on a chi-squared distribution with $\nu = N$-2 degrees of freedom:

$$p\left(\beta_{Y|S_a}|\,\mathbf{D}\right)=\left[\frac{1}{2}\cdot\Gamma\left(\frac{\upsilon}{2}\right)\right]^{-1}\cdot\left(\frac{\upsilon.s^2}{2}\right)^{\frac{\upsilon}{2}}\cdot\beta_{Y|S_a}^{-(\upsilon+1)}\cdot e^{\left(\frac{-\upsilon.s^2}{2.\beta_{Y|S_a}^2}\right)} \quad (8)$$

where s^2 can be calculated from Eq. 2 as linear regression's best-estimate for $\beta_{Y|Sa}$. The posterior joint distribution $\mathrm{p}(\log a,\ b|\beta_{Y|Sa}, \boldsymbol{D})$ can then be expressed as a Normal bi-variate distribution:

$$\begin{cases} p\left(\log a, b|\,\beta_{Y|S_a}, \mathbf{D}\right) = \frac{|X'\cdot X|^{\frac{1}{2}}}{2\pi\beta^2_{Y|Sa}} \mathrm{e}^{\left(\frac{-(\omega-\varpi)'\cdot X'\cdot X\cdot(\omega-\varpi)}{2\cdot\beta^2_{Y|Sa}}\right)} \\ X' = \begin{bmatrix} 1 & 1 & \ldots & 1 \\ \log\left(\mathrm{S}_{a,1}\right) & \log\left(\mathrm{S}_{a,2}\right) & \ldots & \log\left(\mathrm{S}_{a,N}\right) \end{bmatrix} \end{cases} \tag{9}$$

where ϖ is the vector of $[\log a,\ b]$ calculated as the linear least squares best-estimate from regression.

4.1 Estimating the robust fragility curve and its confidence interval by Monte Carlo simulation

The robust fragility curve and its plus/minus one standard deviation confidence interval can be calculated efficiently using Monte Carlo Simulation. This is done by approximating Eqs. 5 and 6 in the following manner:

$$p\left(Y > 1|\, S_a, \mathbf{D}\right) \approx \tilde{R} = \frac{\sum_{i=1}^{n_{\mathrm{sim}}} \Phi\left(\frac{\log \eta_{iY|Sa}}{\beta_{iY|Sa}}\right)}{n_{\mathrm{sim}}} \tag{10}$$

and,

$$\sigma^2_{\chi}\left[F\left(LS|\, S_a, \chi, \mathbf{D}\right)\right] \approx s^2_{\tilde{R}} = \frac{\sum_{i=1}^{n_{\mathrm{sim}}} \left[\Phi\left(\frac{\log \eta_{iY|Sa}}{\beta_{iY|Sa}}\right) - \tilde{R}\right]^2}{n_{\mathrm{sim}}} \tag{11}$$

where n_{sim} is the number of simulations. In above equations, $\eta_{iY|Sa}$ and $\beta_{iY|Sa}$ correspond to the ith realization of the vector of fragility parameters χ_i. The vector χ_i is simulated based on its probability density function $p(\chi|\boldsymbol{D})$ in Eq. 7. This is achieved by first sampling $\beta_{iY|Sa}$ from its (posterior) marginal probability distribution $p(\beta|\boldsymbol{D})$ in Eq. 8. In the next step, conditioning on $\beta_{iY|Sa}$, $\eta_{iY|Sa}$ is sampled form the conditional (posterior) distribution $p(\log a, b|\beta_{Y|Sa}, \boldsymbol{D})$ in Eq. 9. It should be noted that n_{sim} can be a very large value as both the estimators shown in Eqs. 10 and 11 and the probability distributions in Eqs. 8 and 9 are all expressed in a closed and analytic form.

4.2 What is D?

Let vector $\boldsymbol{\Theta}$ represent all the uncertain parameters taken into account in the problem. For example, this vector may contain structural analysis parameters, structural modelling parameters, parameters related to mechanical material properties and parameters related to the ground motion representation. It is enough to note that any given realization θ_i of vector $\boldsymbol{\Theta}$ identifies in a unique manner the structural model and the loading parameters. Ideally, a standard Monte Carlo simulation can be used for generating a set of $i = 1{:}N$ realizations of the vector $\boldsymbol{\Theta}$. It is noteworthy that the different realizations of the vector $\boldsymbol{\Theta}$ need not necessarily be generated from a probability distribution (as in the case of standard Monte Carlo simulation); rather, they need to represent independent observations (e.g., an assumption used in the Bayesian inference in order to derive Eqs. 7 and 8). Therefore, even a set of recorded ground motion time-histories can be included within this vector in order to represent record-to-record variability. For example, the vector θ_i can consist of a specific ground motion time-history in addition to a sample of Monte Carlo realizations for structural modelling parameters.

The set of EDP's and/or decision variables $\boldsymbol{D}$ are obtained in this work as $\boldsymbol{D} = \{Y_i,\ i = 1{:}N\}$ for limit state LS corresponding to the ith realization of the vector of uncertain parameters θ_i. As it will be demonstrated later, the $\boldsymbol{D} = \{Y_i,\ i = 1{:}N\}$ values can be obtained through the Cloud Analysis.

5 Case-study application

A central frame in an existing school (Fig. 1) structure located in Avellino, Italy is considered for the application of the Bayesian Cloud Analysis. The building consists of three main bodies that can be considered structurally separate. Herein, one of the main bodies is considered (Fig. 1a).

5.1 Description of the structural model

The case-study structure consists of three stories with a semi-embedded story and its foundation lies on soil type B. For the structure in question, the original design notes and graphics have been gathered. The building is constructed in the 1960s and it is designed for gravity loads only, as it is frequently encountered in the post second world war construction. In particular the structure is composed of bi-dimensional parallel frames, without transversal beams. The main central frame in the structure is used herein as structural model (Fig. 1b). It should be underlined that considering one of the frames is not intended as a substitute for structural modelling of the entire building.

The columns have rectangular sections with the following dimensions: first storey, $40 \times 55\ \text{cm}^2$, second storey $40 \times 45\ \text{cm}^2$, third storey, $40 \times 40\ \text{cm}^2$, and forth storey, $30 \times 40\ \text{cm}^2$. The beams, also with rectangular section, have the following dimensions: $40 \times 70\ \text{cm}^2$ at first and second storey, and $30 \times 50\ \text{cm}^2$ for the ultimate two floors. The finite element model of the frame is constructed, using the OpenSees software (McKenna et al. 2006), assuming that the non-linear behaviour in the structure is concentrated in plastic hinges (see Jalayer et al. 2013; Elefante et al. 2010 for more information about the structural model). The Beam-with-hinges

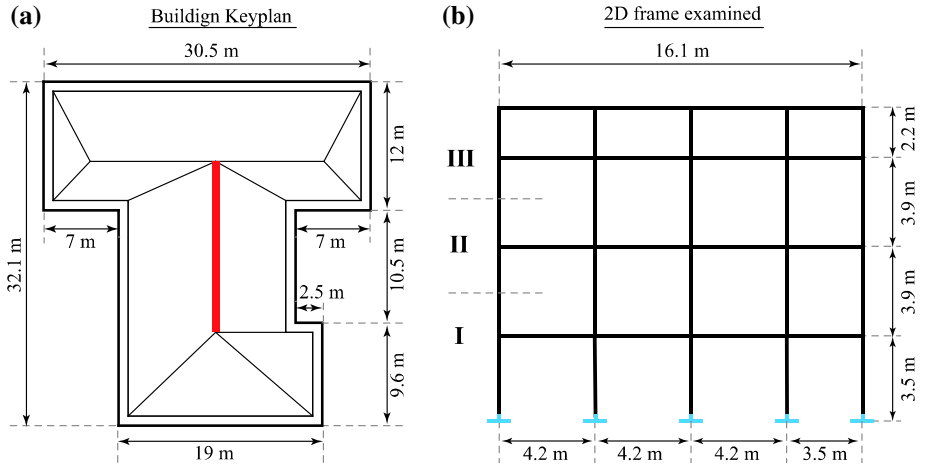

Fig. 1 **a** the school building plan, **b** the 2D bare frame examined in the present study. The *red line* represents the plan view of the examined frame

element is used to model the concentrated plasticity. As the uni-axial material from OpenSees library, Pinching4 is used which is characterized by a quadri-linear backbone and a hysteretic loop. The points on the backbone curve are defined as cracking, yielding, and the peak point, respectively. The coordinates of the peak point are the ultimate bending moment and the 75 % of the ultimate curvature. The first two vibration periods for the considered 2D frame are 0.727 and 0.257 s, and the participation factors at the first and second mode of vibration are equal to 77 and 13 % respectively.

5.2 Characterization of uncertainties

Various sources of uncertainty are taken into account herein; namely: (1) the record-to-record variability in the ground motion conditioned on a fixed value of seismic intensity; (2) the uncertainties in the component capacity models; (3) the uncertainties in mechanical material properties and the structural construction details (stirrup spacing).

5.2.1 Record selection

A set of 20 records (listed below) are selected in order to take into account the record-to-record variability. It should be mentioned that the total number of simulation realizations in the robust fragility method proposed is going to be also equal to 20; that is, the number of records in the set. Out of 20, 18 records are chosen from European Strong Motion Database (Ambraseys et al. 2004) and remaining 2 from the Next Generation Attenuation of Ground Motion Project (Chiou et al. 2008). They are all main-shock free-field recordings and include only one of the horizontal components of the same registration. The soil category on which the ground motions are recorded is stiff soil (400 m/s $< V_{s,30} <$ 700 m/s) which is consistent with the Eurocode 8 (CEN 1998) soil type B (the soil type for the site of the case study structure). The earthquake events have moment magnitude between 5.3 and 7.2, and epicentral distances (ED) ranging between 7 and 87 km. The list of the 20 records is reported in Table 1 below. Figure 2 illustrates the acceleration spectra for the selected ground motion records. Moreover, the median spectrum (the black solid line) and the 16th and 84th percentile spectra (the two black dotted lines) are also plotted in the figure.

5.2.2 The uncertainty in component capacity models

Component capacities are modelled herein as the product of predictive formulas η_{Ci} and unit-median Log Normal variables ε_{Ci} accounting for the uncertainty in component capacity (Jalayer et al. 2007), according to the general format:

$$C_i = \eta_{C_i} \cdot \varepsilon_{C_i} \tag{12}$$

The expression for median capacities corresponding to the considered mechanism are described below. The median chord rotation yielding capacity θ_y for a RC element is based on the study of (Biskinis and Fardis 2010a):

$$\eta_{\theta_y} = \phi_y \cdot \frac{L_s}{3} + 0.0014 \cdot \left(1 + 1.5 \cdot \frac{H}{L_s}\right) + \frac{\phi_y d_b f_y}{8\sqrt{f_c}} \tag{13}$$

where ϕ_y is the yielding curvature, L_s is the shear span, f_c is the concrete strength (MPa), f_y is the steel yield stress (MPa), d_b is the mean diameter of the reinforcement bar and H is

Table 1 The set of 20 ground motions records used in this study

ID	Record	Date	M_W	Fault Mechanism	ED (km)	PGA (g)
1	Valnerina	19/09/1979	5.8	Normal	19	0.04
2	Friuli, Italy-02'	15/09/1976	5.9	Reverse	36	0.21
3	Preveza	10/03/1981	5.4	Thrust	20	0.14
4	Umbria	29/04/1984	5.6	Normal	14	0.21
5	Lazio Abruzzo	07/05/1984	5.9	Normal	15	0.07
6	Etolia	18/05/1988	5.3	Thrust	28	0.04
7	Kyllini	16/10/1988	5.9	Strike slip	20	0.15
8	Irpinia, Italy-01	23/11/1980	6.9	Normal	39	0.13
9	Potenza	05/05/1990	5.8	Strike slip	30	0.10
10	Ano Liosia	07/09/1999	6.0	Normal	11	0.16
11	Adana	27/06/1998	6.3	Strike slip	7	0.03
12	Patras	14/07/1993	5.6	Strike slip	26	0.05
13	Umbria Marche	26/09/1997	6.0	Normal	87	0.52
14	South Iceland	17/06/2000	6.5	Strike slip	48	0.63
15	Duzce 1	12/11/1999	7.2	Oblique	10	0.13
16	Friuli	06/05/1976	6.5	Thrust	18	0.07
17	Campano Lucano	23/11/1980	6.9	Normal	25	0.14
18	Kalamata	13/09/1986	5.9	Normal	19	0.30
19	Montenegro	09/04/1979	5.4	Thrust	36	0.06
20	Tithorea	18/11/1992	5.9	Normal	20	0.03

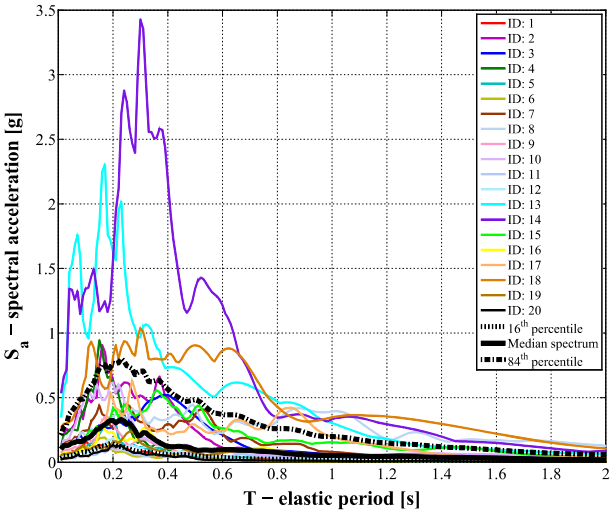

Fig. 2 The acceleration spectra of the selected ground motion records

Table 2 Logarithmic standard deviation values for component capacity models

Unit log-normal variable	β_{Ci}	Literature reference
ε_{Cyield}	0.321	Biskinis and Fardis (2010a)
ε_{Cult}	0.422	Biskinis and Fardis (2010b)
ε_{Cshear}	0.190	De Luca and Verderame (2013)

the section height. The median ultimate chord rotation capacity θ_u of RC members is based on the work of (Biskinis and Fardis 2010b) and is equal to:

$$\eta_{\theta_u} = 0.016 \cdot 0.3^{\upsilon} \cdot \left[\frac{\max\left(0.01, \omega'\right)}{\max\left(0.01, \omega\right)} \cdot f_c\right]^{0.225} \cdot \left[\min\left(9, \frac{L_s}{H}\right)\right]^{0.35} \cdot 25^{\alpha\rho_w \cdot \frac{f_{yw}}{f_c}} \cdot 1.25^{100 \cdot \rho_d} \tag{14}$$

where υ is the normalized axial force, ω and ω' are the tension and compression steel reinforcement ratios, ρ_w is the ratio of transversal reinforcement, f_{yw} is the yield stress of transverse steel, α is the confinement effectiveness ratio and ρ_d is the steel ratio of diagonal bars (if any).

The shear strength is calculated through the Eurocode part 3 (CEN 2005), that is commonly suggested for the assessment of existing buildings under cyclic loads. For the case of shear span ratio (L_S/H) higer than 2 (i.e. slender elements) the median shear strength η_{VRd} is obtained from the following equation:

$$\eta V_{Rd} = V_N + V_C + V_W \tag{15}$$

Where,

$$V_N = \frac{H - x}{2L_s} \cdot \min\left(N, 0.55 \cdot A_c \cdot f_c\right) \tag{16}$$

$$V_C = \left[1 - 0.05 \cdot \min\left(5, \mu_{\Delta,pl}\right)\right] \cdot \left\{0.16 \cdot \max\left(0.5, 100 \cdot \rho_{tot}\right) \cdot \left[1 - 0.16 \cdot \min\left(5, \frac{L_s}{H}\right)\right] \cdot \sqrt{f_c} \cdot A_c\right\} \tag{17}$$

$$V_W = \left[1 - 0.05 \cdot \min\left(5, \mu_{\Delta,pl}\right)\right] \cdot \rho_w \cdot f_{yw} \cdot b \cdot z \tag{18}$$

x is the depth of the neutral axis at yielding, N is the is axial load, A_c is the area of the section, $\mu_{\Delta,pl}$ is the plastic ductility factor (i.e. the chord rotation demand over the yielding chord rotation minus 1, θ/θ_y-1), ρ_{tot} is the total longitudinal reinforcement ratio, b is the section base and z is the internal lever arm. Table 2 illustrates the values of the logarithmic standard deviation β_{Ci} for unit-median Lognormal variables ε_{Ci}. These variables represent the uncertainties in the yielding chord rotation capacity, the ultimate chord rotation capacity, and the ultimate shear capacity.

5.2.3 Uncertainties in the mechanical material properties and the construction details

The parameters identifying the probability distributions for the material mechanical properties (concrete strength and steel yielding force) have been based on the values typical of the post world-war II construction in Italy (Verderame et al. 2001a, b). It is assumed that the material properties are homogeneous across each floor. Table 3 illustrates the parameters that are used to define the lognormal probability distributions for the mechanical material

Table 3 The uncertainties in the material mechanical properties

Material	Type	Median (MPa)	COV	Literature reference
f_{c1}	Log-normal	16.5	0.15	Verderame et al. (2001a)
f_{c2}	Log-normal	16.5	0.15	Verderame et al. (2001a)
f_{c3}	Log-normal	16.5	0.15	Verderame et al. (2001a)
f_y	Log-normal	320	0.08	Verderame et al. (2001b)

Table 4 The uncertainties in the spacing of shear rebar

Defect	Type	Min (mm)	Max (mm)
Beams stirrup spacing	Uniform	150	300
Column stirrup spacing	Uniform	200	350

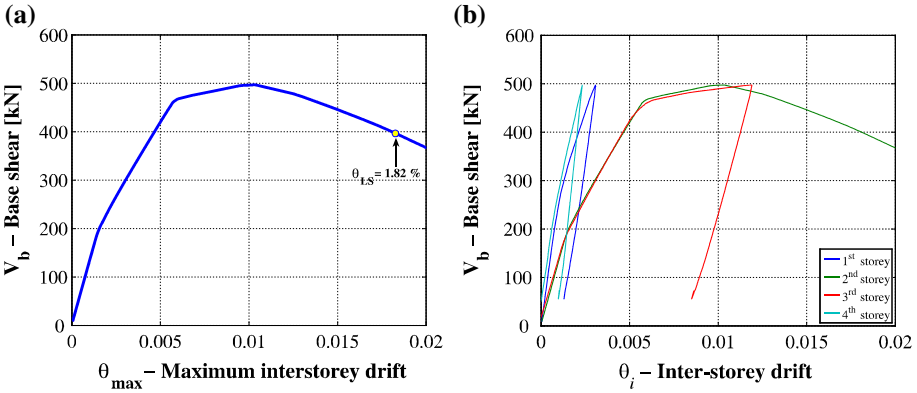

Fig. 3 **a** Pushover curve for the case study structure, **b** the individual storey pushover curves for the four stories

properties; f_{ci} denotes the compression strength for concrete for storey i and f_y denotes the yield strength of steel.

In this study we have considered the shear stirrup spacing in the beams and columns to be the only source of uncertainty related to construction details. Having a presumably shear-critical structure, the spacing of the shear rebar is expected to affect significantly the structural fragility. It is assumed that the information about the shear rebar is limited to knowledge of stirrup diameter (equal to 6 millimetres), and the intervals in which the stirrup spacing is presumed to vary (the minimum values for stirrup spacing are equal to those specified in the original design documents and maximum values are loosely based the maximum admissible stirrup spacing according to the code). Hence, a uniform distribution is assumed in the interval formed by the minimum and the maximum values (Table 4).

5.3 The static pushover results

In order to gain an understanding of the structural behaviour a static pushover analysis has been performed. The results of the pushover analysis are reported as the base shear versus maximum inter-story drift ratio over all the storeys (Fig. 3a). Fig. 3b on the right shows the pushover curve for each storey in terms of base-shear versus storey drift ratio. It can

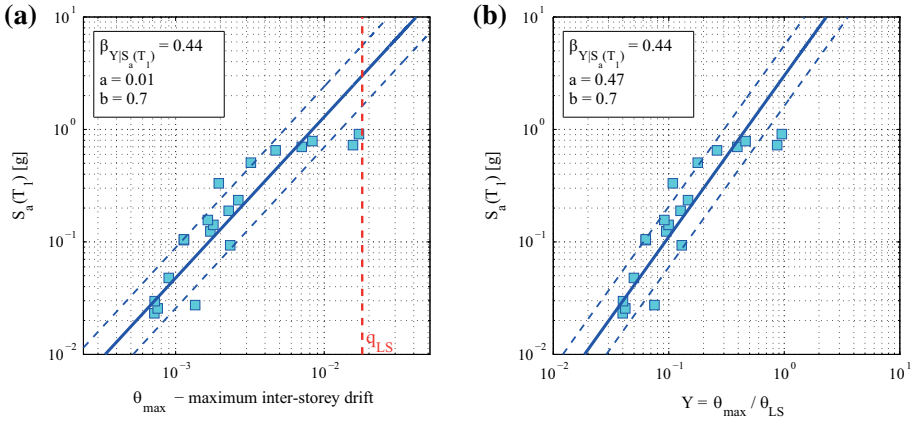

Fig. 4 **a** Cloud Analysis for maximum inter-story drift versus first-mode spectral acceleration. The limit state threshold for global instability is also marked on the figure; **b** Cloud Analysis for maximum inter-story drift normalized with respect to the global instability threshold marked on the pushover curve in Fig. 3a versus first-mode spectral acceleration

be observed that the second floor is the first one to experience large deformations. The pushover curve depicted in Fig. 3a leads also to the evaluation of the maximum inter-storey drift that defines the onset of global instability in the structure. In particular the maximum drift value corresponding to the unloading of 20 % respect to the maximum base-shear value is determined (Panagiotakos and Fardis 2001). As it can be observed from the structural pushover curve in Fig. 3a, the maximum inter-storey drift corresponding to the onset of global stability is equal to 1.82 %. According to the pushover curve, the RC frame has a single story mechanism formed at the second floor. It is worth mentioning that the beginning of the softening branch in the pushover curve in Fig. 3b is determined by the first column plastic hinge of the second floor attaining its peak point at approximately 2 % end rotation. Hence, the onset of global instability in terms of drift is not necessarily equal to the ultimate rotation in the column ends due to the fact that the soft storey mechanism has not yet formed completely at a drift equal to 1.8 % (i.e., at this stage, the hinges are formed only at one of the column ends).

5.4 The Cloud Analysis

Figure 4a illustrates the results of the Cloud Analysis considering only the record-to-record variability for maximum inter-story drift versus first-mode spectral acceleration. The solid lines represent the regression prediction line and the dashed lines represent the regression prediction line plus and minus one logarithmic standard deviation (all in the logarithmic scale). In order to render the results more consistent with those performed for performance variable Y, Fig. 4b illustrates the Cloud Analysis results in terms of maximum inter-story drift normalized with respect to the global stability limit state calculated from the pushover curve in Fig. 3a.

The results obtained using the Cloud Analysis for first-mode spectral acceleration $Sa(T_1)$ and critical demand to capacity ratio Y data pairs are shown in Fig. 5a, b. In particular, Fig. 5a illustrates the results obtained considering only the uncertainties related to the representation of the ground motion (referred to as *case 1*); Fig. 5b illustrates the results considering also the

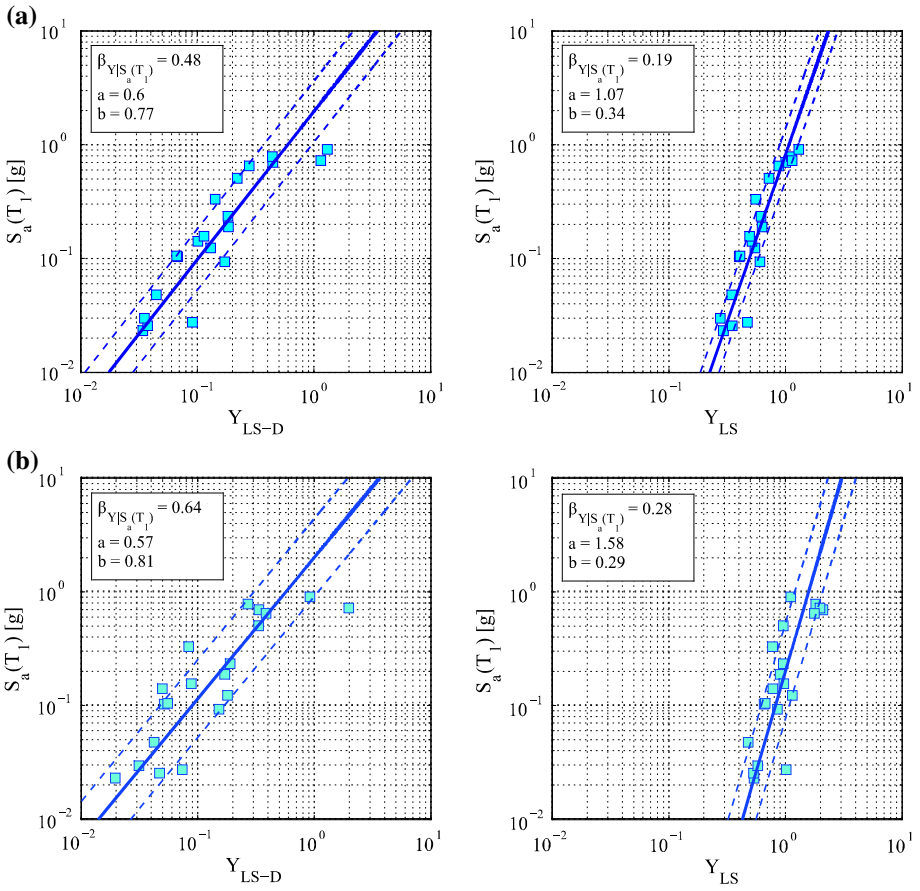

Fig. 5 **a**, **b** Linear regression for cases 1 and 2 considering Y_{LS-D} (*left*) and considering Y_{LS} (*right*)

uncertainties in the structural modelling (material properties plus construction details) and the uncertainties in component capacity models (*case 2*). For each figure described above, the Cloud Analysis presented in the right-hand-side is plotted versus Y_{LS-D} calculated based on cut-sets defined in terms of chord rotation and excluding the fragile (shear-related) cut-sets. This is while the left-hand-side Cloud analyses are plotted versus Y_{LS} calculated over all the considered cut-sets (including also the shear-related ones). It can be observed that the Cloud Analysis results depicted for case 1 in Fig. 4b for maximum inter-story drift (normalized with respect to the limit state threshold for global instability) are very similar to the results illustrated in Fig. 5a(right) for performance variable Y_{LS-D}. This can be seen as an evidence in favour of the maximum inter-story drift as a suitable global response parameter for monitoring excessive chord rotations in the member level.

Several observations can be made by examining the above figures. It can be seen that in almost all cases, the Y_{LS} values (the left-hand figures) reach unity for spectral acceleration values smaller than the spectral acceleration values for Y_{LS-D} (the right-hand figures). The only exceptions are two simulations with soft-storey mechanism for case 1 (only record-to-record variability) and one simulation with soft-storey mechanism for

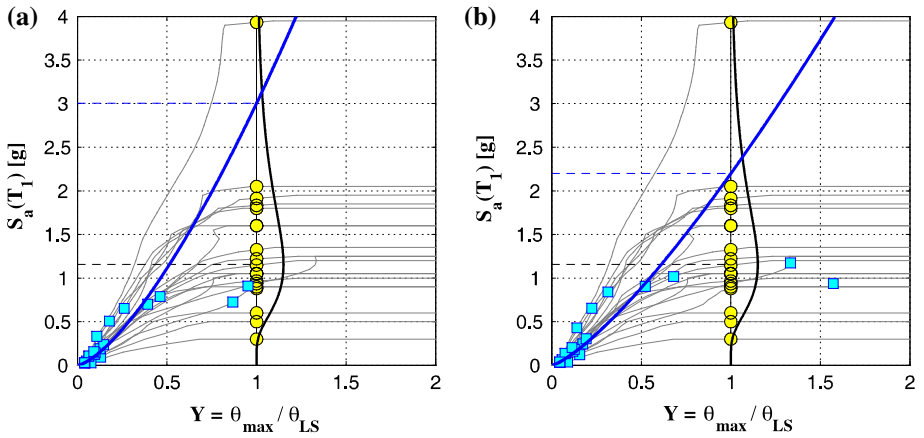

Fig. 6 **a** IDA curves and Cloud Analysis results (data pairs and the power-law regression prediction) for case 1 considering the normalized maximum inter-storey drift as Y; **b** the same results in part (a) overlaid with scaled Cloud Analysis results (scale factor = 1.3)

case 2 (including also the other sources of uncertainty explained in detail beforehand). Moreover, it can be observed that taking into account the structural modelling uncertainties in case 2 (Fig. 5a, b right) leads to an increase in the standard error of regression (dispersion) of Y_{LS} versus spectral acceleration with respect to case 1 (Fig. 5a, b left). It can also be observed that the b-value (the logarithmic slope of the regression line) for Y_{LS} as the dependent variable (around 0.30) shows a marked decrease with respect to when Y_{LS-D} is adopted as the dependent variable (around 0.80). This also signals that the force-dependent cut-sets are more critical with respect to the deformation-based ones.

5.5 The results of the Incremental Dynamic Analysis

The results of the Cloud Analysis are benchmarked with respect to those of the incremental dynamic analysis (IDA) for the same selection of records presented earlier in Sect. 5.2.1. The IDA curves report the change in the performance variable Y for a given ground motion record as a function of the seismic intensity (herein, small-amplitude first-mode spectral acceleration) as the record in question is scaled-up linearly in amplitude. In particular, Fig. 6a illustrates the IDA curves (in thin grey lines) with respect to the maximum inter-story drift (normalized with respect to the global stability limit state threshold) as the EDP. A vertical line plotted at $Y = 1$ demonstrates the dispersion in the spectral acceleration values $S_a^{Y=1}$ (the circles). The figure also demonstrates the (Log Normal) probability density function fitted to the $S_a^{Y=1}$ values (later on represented in the form of a fragility function). The horizontal dashed line represents the median spectral acceleration capacity value from IDA analysis. In order to facilitate the comparison with Cloud Analysis results, the corresponding Cloud data pairs (the squares) and the regression prediction (the thick solid line) from Fig. 4b (considering only record-to-record variability) are also plotted. The spectral acceleration value corresponding to $Y = 1$ from the Cloud regression prediction (around 3g) represents the median spectral acceleration capacity for the limit state considered. The horizontal dashed-dot line represents the median spectral acceleration capacity value from Cloud Analysis. This value can be compared with the median $S_a^{Y=1}$ predicted from the IDA results (around 1.2 g).

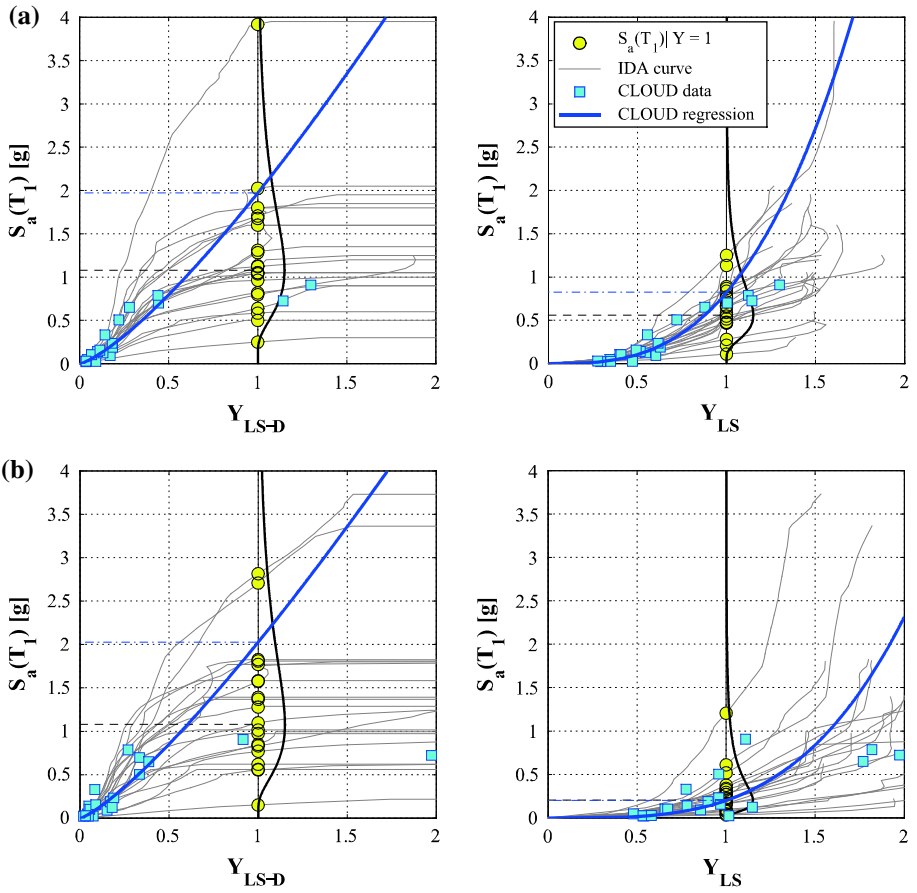

Fig. 7 **a**, **b** IDA curves and Cloud Analysis results (data pairs and the power-law regression prediction) for cases 1 and 2 based on Y_{LS-D} (*right*) and based on Y_{LS} (*left*)

The difference between the results can be attributed to the fact that there are several Cloud data pairs in the range of low S_a and low Y values. On the other hand, there are only two data pairs close to $Y = 1$. This seems to shift the Cloud prediction towards higher spectral acceleration values for $Y = 1$ (i.e., over-estimate the structural capacity). This fact can be appreciated more by looking at Fig. 6b where the same IDA results as that of Fig. 6a are overlaid with the result of the Cloud Analysis for the same set of records but scaled as an ensemble by a factor of 1.3. It can be observed that this shifts more Cloud data pairs away from the origin and reduces the median spectral acceleration capacity estimate for the scaled Cloud Analysis (around 2.2g). However, the regression prediction still seems to be governed by the many data pairs close to the origin. This emphasizes the high sensibility of the Cloud results to the ground motion record selections compared to IDA. In other words, it is quite important to ensure that the ground motion records selected for Cloud Analysis manage to adequately populate the zone of interest (i.e., in this case in the vicinity of $Y = 1$). A rule of thumb would be to have around half of Cloud data points exceeding the limit state threshold ($Y = 1$ herein). Note that pinning down the range of interest with Cloud data pairs might not

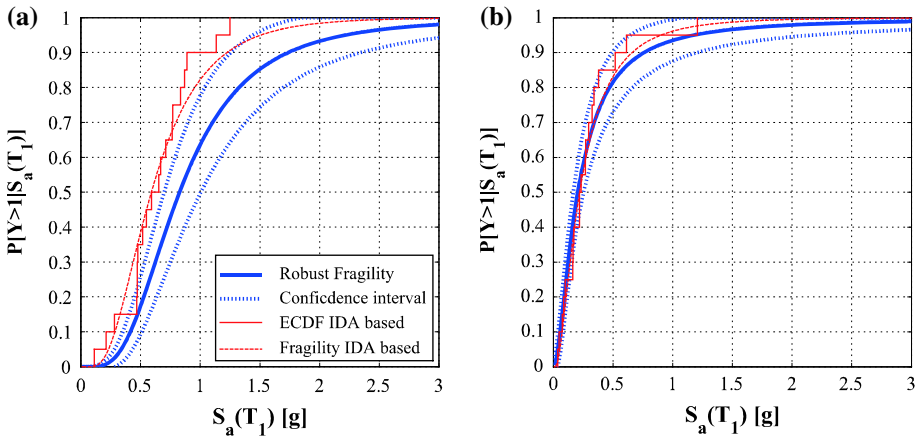

Fig. 8 The robust fragility curves and their plus/minus one standard deviation interval based on **a** case 1; **b** case 2

be achieved with the first round of structural analyses as it might require additional iterations involving scaling or modifications in the set of ground motion records selected.

Figure 7a, b report the IDA results for cases 1 and 2, respectively. The results are presented in the same manner as those of Fig. 6a described in detail above. The figures lined up to the left adopt Y_{LS-D} as a performance variable (and thereby consider the component yield and ultimate chord rotation capacities reported in Sect. 5.2.2). On the other hand, the figures lined up to the right adopt Y_{LS} as the performance variable taking into account also the shear-related cut-sets. It can be observed that the IDA results reported in the right-hand side reveal force-dependent characteristics in the form of IDA curves reaching a fixed threshold instead of the "softening" behaviour common to IDA curves with deformation-based EDP's (e.g., the figures in the right-hand side). It should be noted that in both cases 1 and 2 the IDA results are totally dominated by shear-related cut-sets which is consistent with what observed from Cloud Analysis.

Moreover, it can be seen that the Cloud Analysis results based on Y_{LS} manage to populate more densely the zone of interest (in the vicinity of $Y = 1$). As a result, they lead to median spectral acceleration capacity estimates that are closer to those obtained by the IDA with respect to those based on Y_{LS-D}.

5.6 The robust fragility curves

Figure 8 illustrates the robust fragility curves ($Y = Y_{LS}$) and their plus/minus one standard deviation confidence intervals based on both Cloud Analysis for cases 1 (record-to-record variability) and 2 (including also the uncertainties in material properties and stirrup spacing and the uncertainties in the component capacity models). The robust fragility curves and their confidence intervals are obtained following the procedure described in Sect. 4 for based on Cloud Analysis. The resulting empirical and Log Normal fragility curves obtained based on IDA analysis for the above-mentioned two cases are also potted as thin solid lines and thin dotted lines, respectively.

It can be observed that considering the modelling uncertainties in case 2 leads to an increase in the dispersion of the robust fragility curve. Moreover, it can be observed that the confidence band calculated based on Cloud Analysis fairly manages to capture the empirical

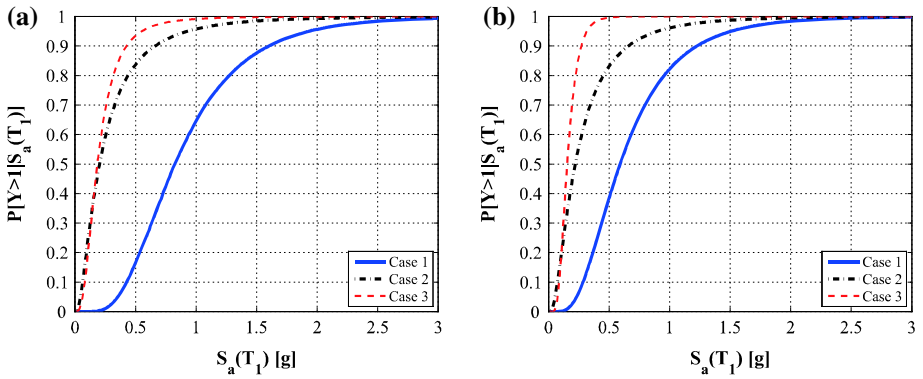

Fig. 9 **a** The robust fragility curves obtained based on Cloud Analysis and **b** the fragility curves IDA based for cases 1 (*solid*), 2 (*dashed*) and 3 (*dashed-dot*)

and Log Normal fragility curves calculated based on IDA. The better match observed for case 2 can be contributed to the fact that the Y values are more concentrated around the zone of interest (Y = 1) with respect to case 1. This can be appreciated by comparing the Cloud results shown in Fig. 7a (right), b (right). It can be presumed that considering the uncertainty in the stirrup spacing is going to lead to a reduction in shear capacity and an overall increase in the Y values.

Figure 9a, b show the robust fragility curves ($Y = Y_{LS}$) obtained based on the Cloud and the IDA-based Log Normal fragility curves, respectively. The figure also depicts a third case where only the record-to-record variability and the structural modelling uncertainties (i.e., the uncertainties in the material mechanical properties and the stirrup spacing) are considered. It can be seen that in cases 2 and 3, considering the capacity modelling uncertainties leads to an increase in the dispersion without significantly shifting the median of the robust fragility curve. Table 5 below summarizes the statistics (median and logarithmic standard deviation for spectral acceleration capacity) for the robust fragility curves calculated based on the Cloud results for cases depicted in Fig. 9. The table also shows the median and logarithmic standard deviation for the Log Normal fragility curve fitted to the IDA results for the above-mentioned three cases. It can be observed that in cases 2 and 3, the robust fragility curves based on Cloud Analysis are closer to the IDA-based fragility curves. The better agreement can be attributed to the fact that considering the structural modelling uncertainties leads to an increase in the Y values (predominantly due to the "one-sided" nature of the uncertainty in the stirrup spacing). Therefore the Cloud data manage to cover more adequately the zone of interest with respect to the base-case where only record-to-record variability is considered.

5.6.1 The effect of the number of records

Figure 10 shows the vertical and horizontal coefficient of variation in fragility estimation denoted by β_H and β_V in the robust fragility calculated at a probability equal to 0.50 as a function of the number of ground motion records. These two metrics are calculated as half of the vertical and horizontal plus and minus one standard deviation confidence interval in Fig. 8 divided by the vertical and horizontal robust fragility components at a probability equal to 0.50. These two metrics are calculated by repeating the procedure for the calculation of the robust fragility based on Cloud Analysis ($Y = Y_{LS}$) for a number of records varying from $n = 4$ to 20. For each n, several combinations of n records from a total of twenty are

Table 5 The statistics (median and logarithmic standard deviation for spectral acceleration capacity) of the robust fragility curves obtained based on Cloud Analysis and the Log Normal fragility curves based on IDA for cases 1, 2 and 3

Case	Cloud (robust fragility)		IDA (Log normal fragility)	
	η	β	η	β
1	0.83	0.56	0.60	0.57
2	0.20	0.96	0.22	0.86
3	0.19	0.65	0.15	0.44

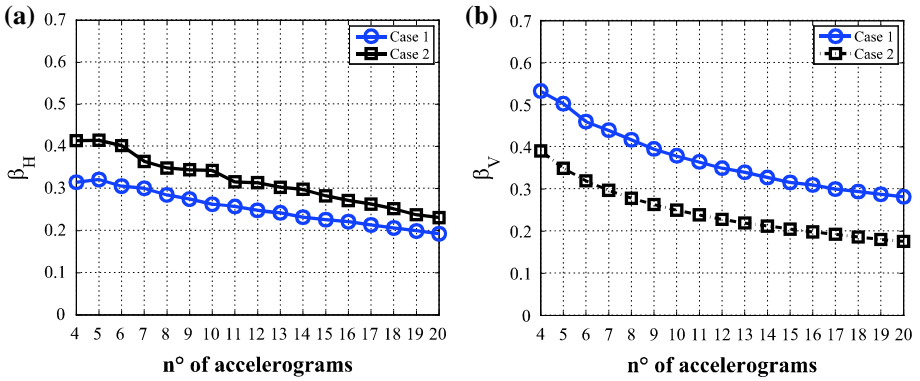

Fig. 10 **a** The horizontal coefficient of variation β_H and **b** vertical coefficient of variation β_V in fragility estimation varying as the number of records

considered. The β_H and β_V values corresponding to each n are plotted versus n in Fig. 10a, b for the cases 1 and 2. It can be observed that both metrics demonstrate a monotonically decreasing trend with respect to the number of records used. As far as it regards the confidence expressed in terms of spectral acceleration (the horizontal coefficient of variation) case 2 seems to have a slightly higher error. However, case 1 seems to have a higher error in terms of confidence measured in probability terms (the vertical coefficient of variation).

6 Conclusions

The Bayesian Cloud Analysis procedure is presented herein as an efficient means for structural fragility assessment using linear regression, taking into account the uncertainty in the parameters of regression. This procedure allows for propagation of the uncertainties both related to record-to-record variability in the ground motion and also the uncertainties related to structural modelling (e.g., the uncertainties in component capacities, in material properties and in construction details) in order to develop "robust fragility" curves. The procedure adopts a global and systemic structural performance variable Y defined based on the reliability "cut-set" concept. The Cloud analyses and the resulting robust fragility curves (together with their confidence intervals) are reported for three cases, record-to-record variability only (*case 1*), record-to-record variability plus the uncertainty in component capacities and the uncertainties in the material properties and stirrup spacing (*case 2*), and record-to-

record variability plus the uncertainties in the material properties and stirrup spacing (*case 3*).

It can be observed from the Cloud Analysis results that the shear-related cut-sets (and not those related to the chord rotation in structural members) are governing the attainment of collapse limit state for the case-study (designed for gravity loading only). The Cloud Analysis results are benchmarked with respect to IDA analyses based on the same selection of ground motion records. In the first place, it can be noted that the IDA curves with respect to the variable Y have a displacement-dependent trend when the shear-related cut-sets are not taken into account. On the other hand, when also the shear-related cut-sets are taken into account, the shape of the IDA curves changes into a force-dependent one. Examining an overlay of the Cloud Analysis results with the IDA results for cases 1 and 2 described above, it can be observed that the Cloud data points manage to replicate the IDA results much better when range of Y values for Cloud data manages to cover the zone of interest (i.e., $Y = 1$). A rule of thumb would be to ensure that around 50 % of the Cloud data have Y values greater than or equal to unity. In fact, the results demonstrate that the when the governing shear-related cut-sets are not taken into account, the majority of Y values are smaller than unity and concentrated close to the origin. In these cases, the IDA and Cloud results do not have a good agreement. This again emphasizes the importance of Cloud data covering the zone of interest. It is also noted that the agreement between the results of Cloud Analysis and IDA is better for cases 2 and 3 when structural modelling uncertainties are also taken into account. This can be attributed to the fact that considering the (undesirable) effect of stirrup spacing leads to consistently larger Y values and as a result manages to cover the zone of interest ($Y = 1$) more adequately. The robust fragility curves based on Cloud Analysis demonstrate a significant decrease in median spectral acceleration capacity and an increase in logarithmic standard deviation of error in cases 2 and 3 respect to case 1 (only record-to-record variability). On the other hand, the robust fragility curves for case 2 (record-to-record variability, material properties and stirrup spacing, and component capacity models) demonstrate a moderate increase in logarithmic standard deviation without shifting significantly the median with respect to case 3 (record-to-record variability plus material properties and stirrup spacing). These observations can be attributed for the most part to the properties of the probability distributions adopted for the significant uncertain parameters. Finally, it can be observed that the relative width of the confidence intervals around the robust fragility curve in cases 1 and 2 has a monotonically decreasing trend with respect to the number of records in the set.

The major limitation to keep in mind for the Bayesian Cloud Analysis presented herein is related to the number and the selection of the ground motion records. As it has been mentioned before, the number of simulation realizations for taking into account structural modelling uncertainties is equal to the number of ground motion records. Hence, studying the relation between the width of the confidence interval and the number of records can provide an estimate of the minimum number of records/realizations needed to achieve a certain level of accuracy. Furthermore, it is important to ensure that the Cloud data points are populating the Y ranges in the vicinity of the value $Y = 1$ for the desired limit state. Finally, as it is generally the case for linear regression, ensuring a wide scatter in the spectral acceleration values of the ground motion records helps in obtaining more statistically significant regression predictions in the Bayesian Cloud Analysis proposed. In other words, with a careful choice of records, the Cloud Method could offer a valid alternative to wide-range methods such as MSA

and IDA in circumstances in which one needs to avoid doing many structural analyses.

Acknowledgments This work was supported in part by the executive Projects ReLUIS-DPC 2013/2014. This support is gratefully acknowledged. The authors would also like to gratefully acknowledge the Guest Editor Christoph Adam and anonymous reviewers for their thorough editing and reviewing of this manuscript.

References

Ambraseys NN, Smit P, Douglas J, Margaris B, Sigbjörnsson R, Olafsson S, Suhadolc P, Costa G (2004) Internet site for European strong-motion data. Bollettino di Geofisica Teorica ed Applicata 45(3):113–129

Baker J (2007) Probabilistic structural response assessment using vector valued intensity measures. Earthq Eng Struct Dyn 36(13):1861–1883

Bazzurro P, Cornell CA, Shome N, Carballo JE (1998) Three proposals for characterizing MDOF non-linear seismic response. ASCE J Struct Eng 124:1281–1289

Beck JL, Au SK (2002) Bayesian updating of structural models and reliability using Markov chain Monte Carlo simulation. J Eng Mech 128(4):380–391

Biskinis D, Fardis MN (2010a) Deformations at flexural yielding of members with continuous or lap-spliced bars. Struct Concr 11(3):127–138

Biskinis D, Fardis MN (2010b) Flexure-controlled ultimate deformations of members with continuous or lap-spliced bars. Struct Concr 11(2):93–108

Box GEP, Tiao GC (1992) Bayesian inference in statistical analysis. Wiley, New York

Celarec D, Dolšek M (2013) The impact of modelling uncertainties on the seismic performance assessment of reinforced concrete frame buildings. Eng Struct 52:340–354

CEN (1998) Comité Européen de normalisation, Eurocode 8: design of structures for earthquake resistance–part 1: General rules, seismic actions and rules for buildings. EN 1:2004

CEN (2005) Comité Européen de normalisation, Eurocode 8: design of structures for earthquake resistance–part 3: assessment and retrofitting of buildings. EN 1998-3, CEN, Bruxels

Chiou B, Darragh R, Gregor N, Silva W (2008) NGA project strong-motion database. Earthq Spectra 24(1):23–44. doi:10.1193/1.2894831

Cornell CA, Krawinkler H (2000) Progress and challenges in seismic performance assessment. PEER Cent News 3(2):1–2

Cornell CA, Jalayer F, Hamburger RO, Foutch DA (2002) The probabilistic basis for the 2000 SAC/FEMA steel moment frame guidelines. ASCE J Struct Eng 128:526–533 Special Issue: Steel Moment Resisting Frames after Northridge Part II

De Luca F, Verderame GM (2013) A practice-oriented approach for the assessment of brittle failures in existing reinforced concrete elements. Eng Struct 48:373–388

Ditlevsen O, Madsen HO (1996) Structural reliability methods. Wiley, New York

Dolsek M (2009) Incremental dynamic analysis with consideration of modeling uncertainties. Earthq Eng Struct Dyn 38(6):805–825

Ebrahimian H, Jalayer F, Asprone D, Lombardi AM, Marzocchi W, Prota A, Manfredi G (2014) A performance-based framework for adaptive seismic aftershock risk assessment. Earthq Eng Struct Dyn (in press). doi:10.1002/eqe.2444

Elefante L, Jalayer F, Iervolino I, Manfredi G (2010) Disaggregation-based response weighting scheme for seismic risk assessment of structures. Soil Dyn Earthq Eng 30(2):1513–1527

Jalayer F (2003) Direct Probabilistic seismic analysis: implementing non-linear dynamic assessments. Ph.D. dissertation, Stanford University, California

Jalayer F, Cornell CA (2003) A technical framework for probability-based demand and capacity factor design (DCFD) seismic formats. Pacific Earthquake Engineering Research Center (PEER) 2003/08

Jalayer F, Franchin P, Pinto PE (2007) A scalar decision variable for seismic reliability analysis of RC frames. Earthq Eng Struct Dyn 36(13):2050–2079

Jalayer F, Cornell CA (2009) Alternative nonlinear demand estimation methods for probability-based seismic assessments. Earthq Eng Struct Dyn 38(8):951–972

Jalayer F, Iervolino I, Manfredi G (2010) Structural modeling uncertainties and their influence on seismic assessment of existing RC structures. Struct Saf 32(3):220–228

Jalayer F, Elefante L, Iervolino I, Manfredi G (2011a) Knowledge-based performance assessment of existing RC buildings. J Earthq Eng 15(3):362–389

Jalayer F, Asprone D, Prota A, Manfredi G (2011b) A decision support system for post-earthquake reliability assessment of structures subjected to after-shocks: an application to L'Aquila earthquake, 2009. Bull Earthq Eng 9(4):997–1014

Jalayer F, Beck JL, Zareian F (2012) Intensity measures of ground shaking based on information theory. ASCE J Eng Mech 138(3):307–316

Jalayer F, De Risi R, Elefante L, Manfredi G (2013) Robust fragility assessment using Bayesian parameter estimation. Paper presented at the Vienna congress on recent advances in earthquake engineering and structural dynamics 2013 (VEESD 2013), Vienna, Austria, 28–30 August

Jaynes ET (2003) Probability theory: the logic of science. Cambridge University Press, Cambridge

Liel AB, Haselton CB, Deierlein GG, Baker JW (2009) Incorporating modeling uncertainties in the assessment of seismic collapse risk of buildings. Struct Saf 31(2):197–211

Luco N, Cornell CA (1998) Seismic drift demands for two SMRF structures with brittle connections. Structural Engineering World Wide; Elsevier Science Ltd, Oxford, England, paper T158-3.

Luco N, Cornell CA (2007) Structure-specific scalar intensity measures for near-source and ordinary earthquake ground motions. Earthq Spectra 23(2):357–392

McKenna F, Fenves GL, Scott MH (2006) OpenSees: open system for earthquake engineering simulation. Pacific Earthquake Engineering Center, University of California, Berkeley, CA

Melchers Robert E (1999) Structural reliability analysis and prediction. Wiley, New York

Panagiotakos TB, Fardis MN (2001) Deformations of reinforced concrete members at yielding and ultimate. ACI Struct J 98(2):135–148

Papadimitriou C, Beck JL, Katafygiotis LS (2001) Updating robust reliability using structural test data. Probab Eng Mech 16(2):103–113

Shome N, Cornell CA, Bazzurro P, Carballo JE (1998) Earthquakes, records, and nonlinear responses. Earthq Spectra 14(3):469–500

Vamvatsikos D, Cornell CA (2002) Incremental dynamic analysis. Earthq Eng Struct Dyn 31(3):491–514

Vamvatsikos D, Fragiadakis M (2010) Incremental dynamic analysis for estimating seismic performance sensitivity and uncertainty. Earthq Eng Struct Dyn 39(2):141–163

Verderame GM, Manfredi G, Frunzio G (2001a) Le proprietà meccaniche dei calcestruzzi impiegati nelle strutture in cemento armato realizzate negli anni 60. X Congresso Nazionale L'ingegneria Sismica in Italia, Potenza-Matera 9–13 Settembre (in Italian)

Verderame GM, Stella A, Cosenza E (2001b) Le propriet meccaniche degli acciai impiegati nelle strutture in cemento armato realizzate negli anni 60. X Convegno Nazionale L'Ingegneria Sismica in Italia, Potenza e Matera 9–13 Settembre (in Italian)